Crashworthiness analysis of empty and foam-filled circular tubes with functionally graded thickness

Barzigar, Seyed Sajad; Ahmadi, Hamed; Liaghat, Gholamhossein; Seidi, Morteza; Mirzaali, Mohammad J.

DOI
10.1007/s40430-024-04781-6

Publication date
2024

Document Version
Final published version

Published in
Journal of the Brazilian Society of Mechanical Sciences and Engineering

Journal of the Brazilian Society of Mechanical Sciences and Engineering (2024) 46:205
https://doi.org/10.1007/s40430-024-04781-6

TECHNICAL PAPER

Crashworthiness analysis of empty and foam-filled circular tubes with functionally graded thickness

Seyed Sajad Barzigar[1] · Hamed Ahmadi[1] · Gholamhossein Liaghat[1,2] · Morteza Seidi[3] · Mohammad J. Mirzaali[4]

Received: 4 November 2023 / Accepted: 8 February 2024

Abstract
Thin-wall structures, particularly thin-walled tubes, play a critical role in load-bearing structures. Enhancing their ability to withstand crushing loads can significantly improve the overall damping efficiency of the system. Functionally graded thickness (FGT) is a promising approach for enhancing the load-bearing properties of thin-walled tubes by enabling control over material usage and localized deformation patterns within the structure. In this study, we proposed a novel theoretical model that analyzes the crushing behavior of hollow and foam-filled FGT thin-walled circular tubes by considering four primary failure mechanisms that contribute to energy dissipation: (1) bending of plastic hinges, (2) membrane stretching, (3) axial foam crushing, and (4) the interaction between foam and the tube's wall. We validated our model against experimental results from previous researchers and observed a good agreement. Additionally, we conduct a comprehensive study to examine the effects of various geometrical parameters, such as power-law functions and normalized wall thickness ratio, on the crushing behavior of FGT structures. Our results demonstrate the accuracy and reliability of our theoretical model and highlight the potential of FGT structures to enhance the performance of thin-walled tubes in a range of load-bearing applications.

Keywords Thin-wall structures · Functionally graded thickness · Theoretical model · Foam-filled tube · Circular tube

1 Introduction

Thin-walled tubes are highly valued for their lightweight and cost-effectiveness, as well as their exceptional energy absorption properties. As a result, they have become a popular choice in a wide range of engineering fields including automotive, aerospace, and railway industries. These structures, known for their exceptional crashworthiness, play a critical role in protecting occupants and vital components from damage in the event of a crash by effectively dissipating the immense impact kinetic energy through various energy absorption mechanisms [1–4].

Several analytical, numerical, and experimental methods have been developed to enhance our understanding of and improve the crashing behavior of these structures under various static or dynamic loading scenarios [5–7]. Other examples of studies on thin-walled structures concern crashing behaviors of holed [8], grooved [9, 10], multicell [11, 12], tapered [13, 14], frusta [15] tubes as well as those with different cross-sectional geometries such as circular [16, 17], triangular [18], rectangular [3, 19], hexagonal [20], corrugated [21], and star-shaped [22] cross sections. A variety of materials, such as steel, aluminum, and composite [23, 24], have been utilized in the development of thin-walled structures with varying cross-sectional geometries. Aluminum circular thin-walled tubes have received considerable attention in numerous studies due to their remarkable deformability, low density, high strength and stiffness, specific energy absorption, and ease of manufacturability [25–27].

Cellular materials and structures, specifically foams and honeycomb structures, have proven to be exceptionally

Technical Editor: João Marciano Laredo dos Reis.

✉ Hamed Ahmadi
h_ahmadi@modares.ac.ir

1 Faculty of Mechanical Engineering, Tarbiat Modares University, Jalal Highway, Tehran, Iran

2 School of Engineering, Computing, and Mathematics, Faculty of Technology, Design, and Environment, Oxford Brookes University, Wheatley Campus, Oxford, UK

3 Department of Mechanical Engineering, University of Texas at San Antonio, San Antonio, Texas, USA

4 Department of Biomechanical Engineering, Faculty of Mechanical, Maritime, and Materials Engineering, Delft University of Technology (TU Delft), Delft, The Netherlands

Published online: 12 March 2024

effective in enhancing the energy absorption characteristics of energy-absorbing structures, including thin-walled structures [28, 29]. By incorporating cellular materials into the cavities of tubular structures, the structure's mass can be kept to a minimum while achieving superior energy absorption performance [30]. This approach is a compelling solution that can greatly enhance the crashworthiness of thin-walled structures and make them a more reliable option for a variety of engineering applications. Among the various filling materials, metallic foams, particularly aluminum foams, have been extensively utilized due to their remarkable ability to undergo plastic deformation at a nearly constant plateau stress [21, 31, 32]. As an example, Hanssen et al. [33, 34] demonstrated that the interaction between the foam filler and the tube wall can result in the energy absorption of the foam-filled tube exceeding the sum of the energies absorbed by the foam and the tube independently. Moreover, the density of the filler material can impact the deformation of the foam-filled tube, resulting in a decrease in the fold length of the structure as the filler density increases [35].

As previously noted, several studies have investigated the energy absorption performance of both empty (E-UT) and foam-filled (F-UT) tubes with "uniform thickness." While these structures have demonstrated favorable energy absorption capacity and crashworthiness, there is potential for further enhancement of their energy absorption performance through the development of structures with "varying wall thickness" [35]. One contributing factor to this potential improvement is the continual advancement of manufacturing technologies, which facilitates the realization of thin-walled tubes with varying thickness.

In recent years, a variety of manufacturing methods have been developed for producing functionally graded thickness (FGT) structures. One such method is tailored-welded blank (TWB) technology, which was initially developed to laser-weld sheet metals with varying materials and thicknesses to create FGT structures. TWB structures have been utilized in a wide range of vehicle components, including the B-pillar [36], door inner panel [37, 38], and vehicle front-end structure [39]. However, a significant drawback of TWB structures is the discontinuous changes in thickness and materials, which can result in high stress concentrations at the geometric and material interfaces. To address this issue, tailor-rolled blank (TRB) technology has been developed, enabling continuous changes in metal thickness by controlling the roller gap [40–42]. Thickness variation in FGT thin-walled structures produced through TWB technology has shown significant effects on their crashworthiness properties [43].

The computational modeling of functionally graded thickness (FGT) thin-walled structures has suggested that tapered and straight FGT tubes exhibit higher energy absorption efficiency under oblique impact loading conditions [44]. This indicates that the energy absorption capacity and crashworthiness performance of FGT tapered circular tubes under axial loading are superior to tapered tubes with uniform thickness [45]. Additionally, circular FGT tubes have demonstrated excellent crashworthiness performance under oblique loading conditions [46]. Overall, FGT tubes have demonstrated better performance than their uniform thickness counterparts under similar loading conditions, with their performance being controllable and even improvable through the proper selection of geometrical parameters [47]. For instance, research has shown that the crashworthiness of thin-walled square tubes can be improved through the use of lateral functionally graded thickness (LFGT) and axial functionally graded thickness (AFGT) [48]. In addition, the implementation of FGT strategies in tube design can alter the collapse mode and crashing performance, particularly under applied oblique loading conditions [49, 50].

Despite the existence of several analytical studies on the energy absorption capacity of empty and foam-filled uniform thickness (UT) tubes, there is currently a significant gap in analytical models available for predicting the energy absorption performance of empty (E-FGT) and foam-filled (F-FGT) circular tubes with thickness variation. Furthermore, there are limited theoretical studies on the crashworthiness of FGT tubes. To address these gaps, we proposed an analytical model to evaluate the energy absorption performance of F-FGT and E-FGT circular tubes. We analyzed the effects of thickness-gradient and eccentricity factor on the crushing behavior of these structures and provided a comprehensive discussion of the results obtained from our novel model. We believe that our proposed model is a crucial step forward in developing a comprehensive understanding of the crashworthiness of FGT structures and optimizing their design for enhanced safety and crash performance.

2 Definition of the crashworthiness parameters

In the field of engineering, evaluating the crashworthiness of thin-walled structures involves calculating crashworthiness parameters by analyzing the load–displacement curve under axial compression [51]. Mean crushing force (MCF), energy absorption (EA), and specific energy absorption (SEA) are essential metrics used to compare the energy absorption performance of different structures. Below are the definitions of these parameters, which are considered fundamental tools in assessing the crashworthiness of thin-walled structures.

EA is equal to the area under the load–displacement curve in which the elastic deformation is neglected and can be calculated as:

$$\mathrm{EA} = \int_0^{\delta} F(\delta)\mathrm{d}\delta \tag{1}$$

where $F(\delta)$ is the momentary crushing force and δ is the corresponding applied displacement.

SEA is referred to as the absorbed energy per unit mass and is defined as:

$$\mathrm{SEA} = \frac{\mathrm{EA}}{M} \tag{2}$$

where M is the total mass of the crushed section of the structure. Actually, SEA shows the efficiency of the structure [52].

MCF shows the capacity of the structure in absorbing energy under a given displacement and can be written as:

$$\mathrm{MCF} = \frac{\mathrm{EA}}{\delta} \tag{3}$$

Figure 1 illustrates the typical force–displacement curve of circular tubes with a uniform thickness (UT) and a functionally graded thickness (FGT) under quasi-static compressive loading. These curves exhibit the distinctive structural behavior and performance of UT and FGT tubes under comparable compressive loading conditions. Notably, as the displacement increases, UT tubes maintain a nearly constant force value, while FGT tubes experience an increase in crushing force values due to the variation of local stiffnesses along their length.

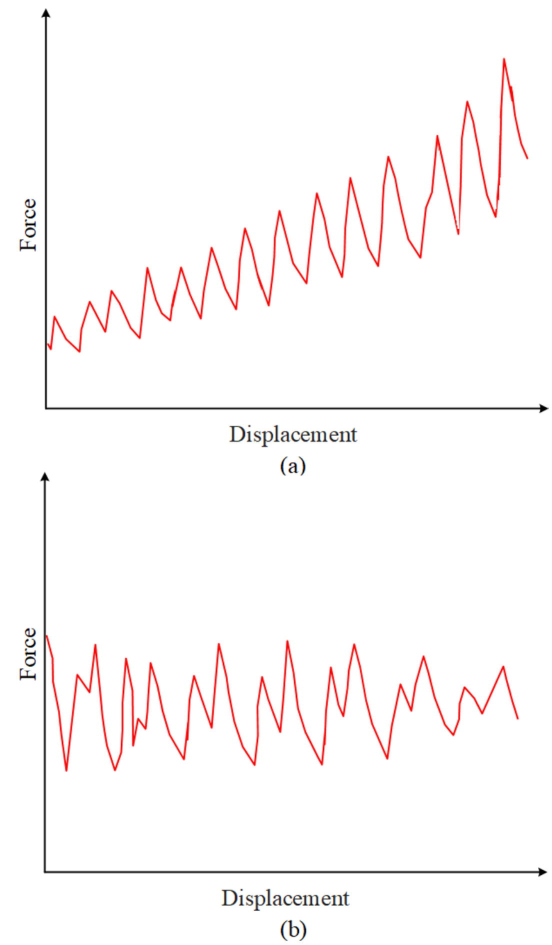

Fig. 1 The typical force–displacement curve of **a** FGT and **b** UT tube under uniaxial compression loading

3 Theoretical analysis

3.1 Theoretical model

The present study introduces an analytical model for E-FGT and F-FGT circular tubes, incorporating the concept of super folding elements. The model is built upon the assumption that these tubes exhibit axisymmetric deformation under uniaxial loading conditions [53]. In contrast to asymmetric deformation, axisymmetric deformation is characterized by uniform changes in shape and displacement occurring in all directions around a central axis. This deformation mode ensures symmetrical and consistent behavior along the loading axis. By assuming axisymmetric deformation under uniaxial loading conditions, our model considers that the tubes will uniformly deform around their central axis when subjected to a load applied in a single direction. This assumption serves as the foundation of our analytical model, which effectively utilizes the super folding elements. We applied this model to forecast the crashworthiness of E-FGT and F-FGT circular tubes with various thickness patterns and compared the outcomes with UT structures having the same mass. To consider the interaction between the tube wall and the foam material in the foam-filled tube, we followed the analytical approach recommended in [32, 54, 55].

Figure 2 shows the schematic of different structural configurations studied in this paper. The thickness gradient function $t(x)$ of the E-FGT and F-FGT circular tube was defined by the power-law function proposed by Sun et al. [51]:

$$t(x) = t_{\min} + \left(t_{\max} - t_{\min}\right)\left(\frac{x}{H}\right)^n \tag{4}$$

where x is the distance from the top end of the tube, $t_{\min}$ and $t_{\max}$ are the minimum and maximum thickness of the tube, H denotes the total height of the FGT tube, and n is the power-law exponent varying between 0.2 and 10 (Fig. 3a). In case, the power-law exponent's value is less than 1, the thickness pattern of the FGT tube wall takes on a convex shape, whereas for values greater than 1, it becomes concave (as shown in Fig. 3a). Therefore, increasing the grading

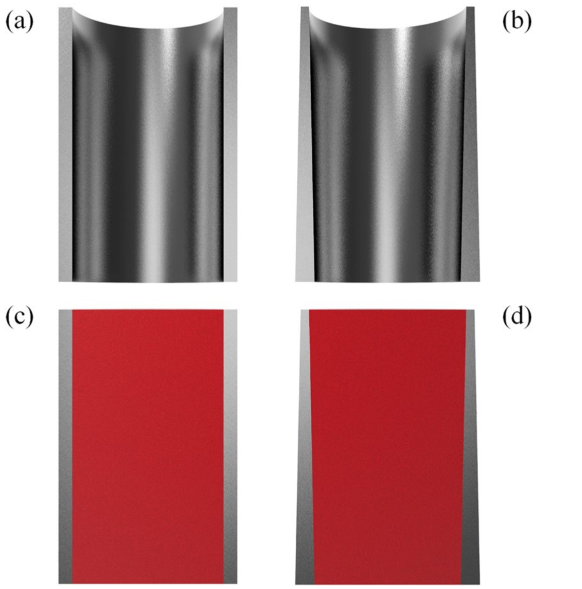

Fig. 2 A schematic of tubes with different structural configurations, **a** An empty tube with uniform thickness (E-UT), **b** An empty tube with functionally graded thickness (E-FGT), **c** A foam-filled tube with uniform thickness (F-UT), **d** A foam-filled tube with functionally graded thickness (F-FGT)

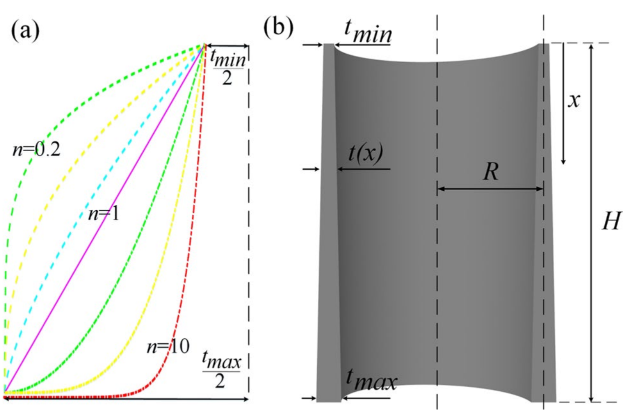

Fig. 3 **a** Different thickness patterns resulted from varying the coefficient of exponents in Eq. 4, **b** Geometric model of the FGT circular tube with $n = 1$

exponent results in a reduction in the overall mass of the structure.

For given values of $t_{\max}$, $t_{\min}$, and power-law exponent, n, an equivalent uniform thickness for a circular UT tube (t_U) with the same mass can be calculated as [44]:

$$t_U = t_{\min} + \frac{t_{\max} - t_{\min}}{n + 1} \tag{5}$$

Figure 4 displays the alterations in normalized thicknesses ($t_U/t_{\min}$, $t_{\max}/t_{\min}$) concerning various coefficients

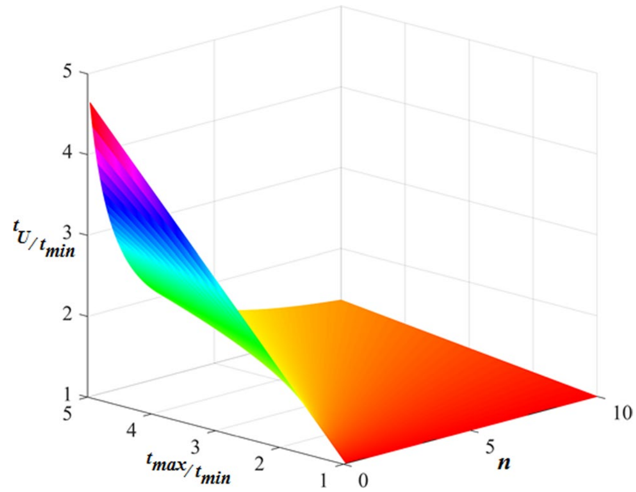

Fig. 4 The relation between the normalized wall thicknesses (i.e., $t_U/t_{\min}$, $t_{\max}/t_{\min}$) and the values of the grading exponent, n, in Eq. 5, in UT and FGT tubes

of the power-law function in UT and FGT tubes. Figure 4 indicates that, for a specific value of $t_{\max}$ and $t_{\min}$, elevating the grading exponent n leads to a reduction in wall thickness in UT tubes.

The super folding element suggests that a complete folding cycle of a model can be divided into two key parts, as shown in Fig. 5: First, the outward buckling, which initiates at plastic hinge A and concludes at plastic hinge C. Second, the inward buckling, which occurs after the outward buckling (step 1) and starts at plastic hinge C and ends at plastic hinge D. It is worth noting that in the presented model, the elastic deformation of the tube and foam material has a minimal impact and is therefore considered negligible which means that the material model assumes both the tube and foam to be ideal fully plastic [8, 56].

To maintain the energy equilibrium in the structure during the folding cycle, the input force is gradually dissipated through progressive folding. As a result, the external work performed by the input force is converted into plastic strain energy within the material. Consequently,

$$2h\eta P_{\mathrm{m}} = E_{\mathrm{tot}} \tag{6}$$

where P_{m} represents the mean crushing force, h is the half of the crushing fold, η is the effective crushing distance factor [57], and E_{tot} denotes the total energy absorbed by the F-FGT circular tube. This absorbed energy is defined as the algebraic sum of four energy components: (1) the energy dissipated in bending deformation (E_b), (2) the energy dissipated in the membrane deformation (E_{m}), (3) the energy dissipated in the crushing of the foam (E_{foam}), and (4) the energy dissipated due to the interaction effect between the foam material and the tube wall (E_{inter}):

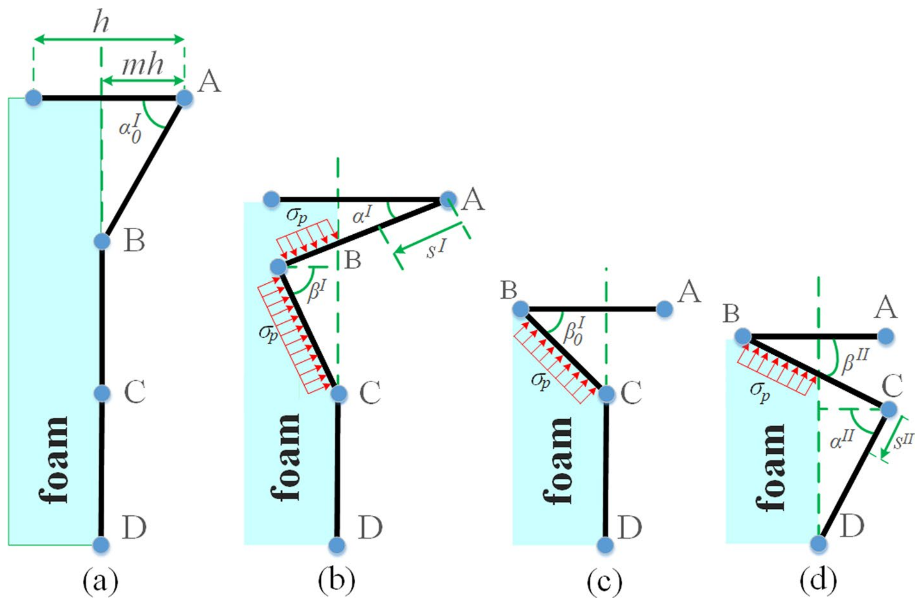

Fig. 5 Different stages of a complete (inward (**a**, **b**) and outward (**c**, **d**)) folding cycles in a super folding element in foam-filled circular tubes

$$E_{\text{tot}} = E_{\text{m}} + E_b + E_{\text{foam}} + E_{\text{inter}} \tag{7}$$

The total energy absorbed by an empty circular tube (E-FGT) can then be given as:

$$E_{\text{shell}} = E_{\text{m}} + E_b \tag{8}$$

As shown in Fig. 5, during a complete folding cycle, the initial outward angle, $\boldsymbol{\alpha}_0^{\boldsymbol{I}}$, and the initial inward angle, $\boldsymbol{\beta}_0^{\boldsymbol{II}}$, are related to the eccentricity factor $\boldsymbol{m}$ [53], which describes the eccentricity of the folding process. Thus, it can be assumed that,

$$\cos\alpha_0^{\text{I}} = m$$

$$\cos\beta_0^{\text{II}} = 1 - m \tag{9}$$

3.2 Membrane energy

As the structure undergoes outward and inward folding, the tube material between adjacent plastic hinges will experience compression and extension, respectively (as shown in Fig. 5). The membrane energy increment of the tube material can be expressed as:

$$dE_{\text{m}} = \int_{s_{\text{m}}} N_{\text{p}} |d\varepsilon_\theta| \mathrm{d}s_{\text{m}} \tag{10}$$

where s_{m}, N_{p}, and $\mathrm{d}\varepsilon_\theta$ are respectively the area of deformation zone, fully plastic membrane force per unit circumferential length, and the mean engineering strain increment. As shown in Fig. 3b, the thickness of the FGT tube wall at any point is related to the axial distance of that point from the top end of the tube. The fully plastic membrane force per unit circumferential length (N_{p}) in any point with a distance of x from the top end can be given as:

$$N_{\text{p}} = \sigma_0 t(x) \tag{11}$$

where σ_0 is the flow stress of the tube material and can be given as [16, 32]:

$$\sigma_0 = \sqrt{\frac{\sigma_y \sigma_u}{1 + k}} \tag{12}$$

k is the strain hardening exponent, σ_y is the yield stress, and σ_u is the ultimate stress of the tube constituent material. Mean engineering strain increment ($d\varepsilon_\theta$) can be expressed as:

$$d\varepsilon_\theta = \frac{dr}{R} \tag{13}$$

where dr is the radial displacement increment, and as shown in Fig. 3b R is the mean radius of the FGT tube. Membrane energy increment of the first part (I) of the folding cycle is given by:

$$dE_{\text{m}}{}^{\text{I}} = 2\pi R\sigma_0 \int_{S^{\text{I}}} [t(S^{\text{I}} + h^*) \frac{|\mathrm{d}r_{AB}^{\text{I}}|}{R} + t(S^{\text{I}} + h + h^*) \frac{|\mathrm{d}r_{BC}^{\text{I}}|}{R}] \mathrm{d}S^{\text{I}} \tag{14}$$

where, S^{I} is the coordinate along the length direction of the fold's arm, and h^* is the algebraic sum of the previous folding crush lengths of the FGT tube. dr_{AB}^{I} and dr_{BC}^{I} are the radial displacement increment of AB and BC fold's arm in the first part of the folding cycle, which can be expressed as [8]:

$$\begin{cases} r_{AB}^{\mathrm{I}} = S^{\mathrm{I}}\cos\alpha^{\mathrm{I}} - mh \\ dr_{AB}^{\mathrm{I}} = -S^{\mathrm{I}}\sin\alpha^{\mathrm{I}}(-d\alpha^{\mathrm{I}}) \end{cases} \tag{15}$$

and

$$\begin{cases} r_{BC}^{\mathrm{I}} = S^{\mathrm{I}}\cos\beta^{\mathrm{I}} \\ dr_{BC}^{\mathrm{I}} = -S^{\mathrm{I}}\sin\beta^{\mathrm{I}}(-d\beta^{\mathrm{I}}) \end{cases} \tag{16}$$

During the first part of a folding cycle, angle α^{I} changes from α_0^{I} to 0 and the angle β^{I} changes from $\pi/2$ to β_0^{II}. By inserting Eqs. (15) and (16) into Eq. (14) and by integrating over S^{I} (from 0 to h), α^{I} (from α_0^{I} to 0) and β^{I} (from $\pi/2$ toβ_0^{II}), membrane energy of the first part is obtained by:

$$E_{\mathrm{m}}{}^{\mathrm{I}} = 2\pi\sigma_0\left[\int_{\alpha_0^{\mathrm{I}}}^{0}\sin\alpha^{\mathrm{I}}\mathrm{d}\alpha^{\mathrm{I}}\right][\int_0^h\left(2t_{\min} + \left(t_{\max} - t_{\min}\right)\right. \left.\left(\left(\frac{S^{\mathrm{I}} + h^*}{H}\right)^n + \left(\frac{S^{\mathrm{I}} + h + h^*}{H}\right)^n\right)\right)(-S^{\mathrm{I}})\mathrm{d}S^{\mathrm{I}}] \tag{17}$$

For the second part of the folding cycle, membrane energy increment can be expressed as:

$$dE_{\mathrm{m}}{}^{\mathrm{II}} = 2\pi R\sigma_0\int_{S^{\mathrm{II}}}[t(S^{\mathrm{II}} + h + h^*)\frac{\left|dr_{BC}^{\mathrm{II}}\right|}{R} + t(S^{\mathrm{II}} + 2h + h^*)\frac{\left|dr_{BC}^{\mathrm{II}}\right|}{R}]\mathrm{d}S^{\mathrm{II}} \tag{18}$$

where

$$\begin{cases} r_{BC}^{\mathrm{II}} = S^{\mathrm{II}}\cos\beta^{\mathrm{II}} - (1-m)mh \\ dr_{BC}^{\mathrm{II}} = -S^{\mathrm{II}}\sin\beta^{II}\left(-d\beta^{\mathrm{II}}\right) \end{cases}, \tag{19}$$

and

$$\begin{cases} r_{CD}^{\mathrm{II}} = S^{\mathrm{II}}\cos\alpha^{\mathrm{II}} \\ dr_{CD}^{\mathrm{II}} = -S^{\mathrm{II}}\sin\alpha^{II}(-d\alpha^{\mathrm{II}}) \end{cases} \tag{20}$$

during the second part of a folding cycle, α^{II} and β^{II} respectively change from $\pi/2$ to α_0^{I} and from β_0^{II} to 0. Inserting Eqs. (19) and (20) into Eq. (18) and by integrating over S^{II} (from 0 to h), α^{II} (from $\pi/2$ to α_0^{I}) and β^{II} (from β_0^{II} to 0), the membrane energy of the second part of a folding cycle can be defined as:

$$E_{\mathrm{m}}{}^{\mathrm{II}} = 2\pi\sigma_0\left[\int_{\beta_0^{\mathrm{II}}}^{0}\sin\beta^{II}\mathrm{d}\beta^{\mathrm{II}}\right][\int_0^h\left(2t_{\min} + \left(t_{\max} - t_{\min}\right)\right. \left.\left(\left(\frac{S^{\mathrm{I}} + h + h^*}{H}\right)^n + \left(\frac{S^{\mathrm{I}} + 2h + h^*}{H}\right)^n\right)\right)(-S^{\mathrm{II}})\mathrm{d}S^{\mathrm{II}} \tag{21}$$

By summing up the Eqs. (17) and (21), the energy dissipated due to the membrane deformation of FGT tube can be expressed as:

$$E_{\mathrm{m}} = E_{\mathrm{m}}{}^{\mathrm{I}} + E_{\mathrm{m}}{}^{\mathrm{II}} \tag{22}$$

By ignoring the thickness variation in FGT tube ($t_{\min} = t_{\max}$), Eq. (22) will simplify to:

$$E_{\mathrm{m}} = 2\pi N_{\mathrm{p}}h^2 \tag{23}$$

which is the same as the UT tube membrane energy equation under axial loading, proposed in [53].

3.3 Bending energy

Bending energy of the FGT tube wall can be divided into two separate sections: (1) energy dissipated by plastic hinges A, B, and C in the first part of the folding process, which is controlled by the angle α and (2) the energy dissipated by plastic hinges B, C and D in the second part of the folding process which is controlled by the angle β. When determining the absorbed energy by the plastic hinges, it is assumed that there is no interaction between the bending moment and membrane force of the tube material. During a complete folding cycle, bending energy increment of the FGT tube is given by:

$$dE_b = \frac{\pi}{2}\sum_{i=1}^{z}\sigma_0 t_i^2 R_i\left|d\theta_i\right| \tag{24}$$

where R_i, $d\theta_i$, and t_i are radial distance, the relative rates of rotation, and FGT tube wall thickness, respectively, at the ith hinge. As shown in Fig. 5a, b, plastic hinges A, B, and C are the only active hinges during the first part of the folding process. Thus, bending energy increment of the first part of the folding process of the FGT tube can be expressed as:

$$dE_b{}^{\mathrm{I}} = \frac{\pi}{2}\sigma_0\left((t_A^{\mathrm{I}})^2 R_A{}^{\mathrm{I}}\left|d\theta_A{}^{\mathrm{I}}\right| + (t_B^{\mathrm{I}})^2 R_B{}^{\mathrm{I}}\left|d\theta_B{}^{\mathrm{I}}\right| + (t_C^{\mathrm{I}})^2 R_C{}^{\mathrm{I}}\left|d\theta_C{}^{\mathrm{I}}\right|\right) \tag{25}$$

where

$$\left|d\theta_A{}^{\mathrm{I}}\right| = -d\alpha^{\mathrm{I}}, R_A{}^{\mathrm{I}} = R + mh, t_A{}^{\mathrm{I}} = t_{\min} + \left(t_{\max} - t_{\min}\right)\left(\frac{h^*}{H}\right)^n \tag{26a}$$

$$\left|d\theta_B{}^{\mathrm{I}}\right| = -d\alpha^{\mathrm{I}} - d\beta^{\mathrm{I}}, R_B{}^{\mathrm{I}} = R + mh - h\cos\alpha^{\mathrm{I}}, t_B{}^{\mathrm{I}} = t_{\min} + \left(t_{\max} - t_{\min}\right)\left(\frac{h + h^*}{H}\right)^n \tag{26b}$$

$$\left|d\theta_C{}^{\mathrm{I}}\right| = -d\beta^{\mathrm{I}}, R_C{}^{\mathrm{I}} = R, t_C{}^{\mathrm{I}} = t_{\min} + \left(t_{\max} - t_{\min}\right)\left(\frac{2h + h^*}{H}\right)^n \tag{26c}$$

During the second part of the folding cycle, plastic hinges B, C, and D are active, and the bending energy increment of the second part of the folding process of the FGT tube can be defined as:

$$dE_b{}^{\mathrm{II}} = \frac{\pi}{2}\sigma_0\left((t_B^{\mathrm{II}})^2 R_B{}^{\mathrm{II}}\left|d\theta_B{}^{\mathrm{II}}\right| + (t_C^{\mathrm{II}})^2 R_C{}^{\mathrm{II}}\left|d\theta_C{}^{\mathrm{II}}\right| + (t_D^{\mathrm{II}})^2 R_D{}^{\mathrm{II}}\left|d\theta_D{}^{\mathrm{II}}\right|\right) \tag{27}$$

where

$$\left|d\theta_B{}^{\mathrm{II}}\right| = -d\beta^{\mathrm{II}}, R_B{}^{\mathrm{II}} = R - h(1-m),$$
$$t_B{}^{\mathrm{II}} = t_{\min} + \left(t_{\max} - t_{\min}\right)\left(\frac{h + h^*}{H}\right)^n \tag{28a}$$

$$\left|d\theta_C{}^{\mathrm{II}}\right| = -d\alpha^{\mathrm{II}} - d\beta^{\mathrm{II}}, R_C{}^{\mathrm{II}} = R - h(1-m) + h\cos\beta^{\mathrm{II}},$$
$$t_C{}^{\mathrm{II}} = t_{\min} + \left(t_{\max} - t_{\min}\right)\left(\frac{2h + h^*}{H}\right)^n \tag{28b}$$

$$\left|d\theta_D{}^{\mathrm{II}}\right| = -d\alpha^{\mathrm{II}}, R_D{}^{\mathrm{II}} = R, t_D{}^{\mathrm{II}} = t_{\min} + \left(t_{\max} - t_{\min}\right)\left(\frac{3h + h^*}{H}\right)^n \tag{28c}$$

By inserting Eqs. (26) and (28) into Eqs. (25) and (27) and integrating over α^{I} (from α_0^{I} to 0), β^{I} (from $\pi/2$ to β_0^{II}), α^{II} (from $\pi/2$ to α_0^{I}) and β^{II} (from β_0^{II} to 0), bending energy of the FGT circular tube can be obtained by:

$$E_b = E_b{}^{\mathrm{I}} + E_b{}^{\mathrm{II}} \tag{29}$$

3.4 Foam energy

By disregarding the effect of Poisson's ratio of the foam material ($\upsilon = 0$), dissipated energy by the foam filler in a F-FGT tube can be simply calculated by the following equation:

$$E_{\mathrm{foam}} = \pi\sigma_{\mathrm{p}}\left[\int_0^{2h\eta}\left(R - \frac{\left[t_{\min} + \left(t_{\max} - t_{\min}\right)\left(\frac{\frac{s}{\eta} + h^*}{H}\right)^n\right]}{2}\right)^2 \mathrm{d}s\right] \tag{30}$$

where σ_{p} is the plateau stress of the foam material, which is nearly constant, and ds is the displacement increment in the longitudinal direction.

3.5 Interaction energy

The interaction between the foam filler and the tube wall can be simplified as a uniform pressure, which is equal to the plateau stress of the foam material (σ_{p}). This pressure is applied to the inward part of the fold [8, 32, 55], and the interfacial friction can be neglected. Furthermore, in the proposed model, the effect of the thickness gradient of the inside wall of the FGT tube is ignored due to its small contribution and to obtain a concise expression for the interaction energy. In the first part of the folding process, a uniform pressure is applied to arms AB and BC, whereas in the second part of the process, the pressure is only applied to arm BC [8]. During a complete folding cycle, interaction energy increments can be expressed as:

$$\mathrm{d}E^{\mathrm{I}}{}_{\mathrm{inter},AB} = 2\pi\sigma_{\mathrm{p}}\int_{\frac{mh}{\cos\alpha^{\mathrm{I}}}}^{h} S^{\mathrm{I}}\left(R - S^{\mathrm{I}}\cos\alpha^{\mathrm{I}} + mh\right)\mathrm{d}S^{\mathrm{I}}\left(-d\alpha^{\mathrm{I}}\right) \tag{31}$$

$$\mathrm{d}E^{\mathrm{I}}{}_{\mathrm{inter},BC} = 2\pi\sigma_{\mathrm{p}}\int_0^{h} S^{\mathrm{I}}\left(R - S^{\mathrm{I}}\cos\beta^{\mathrm{I}}\right)\mathrm{d}S^{\mathrm{I}}\left(-d\beta^{\mathrm{I}}\right) \tag{32}$$

$$\mathrm{d}E^{\mathrm{II}}{}_{\mathrm{inter},BC} = 2\pi\sigma_{\mathrm{p}}\int_{\frac{mh}{\cos\alpha^{\mathrm{I}}}}^{h} S^{\mathrm{II}}\left(R - S^{\mathrm{II}}\cos\beta^{\mathrm{II}} - (1-m)h\right)\mathrm{d}S^{\mathrm{II}}\left(-d\beta^{\mathrm{II}}\right) \tag{33}$$

Summing up the interaction energy increments and by integrating the result, the energy absorbed due to interaction between the tube wall and the foam material can be obtained by:

$$E_{\mathrm{inter}} = \pi\sigma_{\mathrm{p}}(Rh^2C_1(m) - h^3C_2(m)) \tag{34}$$

where $C_1(m)$ and $C_2(m)$ are the first and the second interaction coefficient defined in this study, respectively. Both $C_1(m)$ and $C_2(m)$ are functions of eccentricity factor m and can be expressed as:

$$C_1(m) = \frac{\pi}{2} + \arccos(m) - \arccos(1-m) + (1-m)\sqrt{m(2-m)} - m\sqrt{(1-m)(1+m)} \tag{35}$$

$$C_2(m) = \frac{2}{3} + m(\arccos(m)) + \frac{\left(2 - 5m^2\right)}{3}\sqrt{1-m^2} + \sqrt{m(2-m)} - \frac{5}{3}\sqrt{(m(2-m))^3} \tag{36}$$

3.6 Total dissipated energy and mean crushing force during each fold

By substituting Eqs. (22), (29), (30), and (34) into Eqs. (8) and (7), the total energy absorbed in E-FGT and F-FGT tubes during a complete folding cycle can be calculated. According to Eq. (6) and the energy equilibrium, the mean crushing force of F-FGT tubes during each folding process can be determined as:

$$P_{\mathrm{m}} = \frac{E_{\mathrm{tot}}}{2h\eta} \tag{37}$$

and the mean crushing force of E-FGT tubes during a complete folding cycle can be obtained by:

$$P_{\text{shell}} = \frac{E_{\text{shell}}}{2h\eta} \tag{38}$$

where η is the effective crushing distance factor. When analyzing tube materials that exhibit significant strain hardening, it is widely recognized that the effective crushing distance factor (η) is a crucial parameter to consider. Specifically, in such cases, η is typically found to be within the range of 0.7 to 0.75. However, if the strain hardening effect in the tube material is not significant, then the value of η can be assumed to be equal to 1. By minimizing Eqs. (37) and (38) with respect to h, half of the crushing fold in each fold cycle of F-FGT and E-FGT tube can be determined, respectively. By inserting the calculated values in Eqs. (37) and (38), the crushing force for completing each folding step of F-FGT or E-FGT tubes can be determined.

4 Result and discussion

4.1 Validation of the theoretical model

To validate our analytical approach for E-FGT and F-FGT circular tubes, we compared our results with experimental data presented in [49]. To ensure a fair comparison, we selected similar geometry (i.e., $R = 30$ mm, $H = 180$ mm) and material (i.e., $\sigma_0 = 104$ MPa) as those used in [49]. The FGT tubes in [49] had a linearly variable thickness ($n = 1$), with a minimum thickness of 1 mm and a maximum thickness of 3 mm. The UT tube wall had a uniform thickness of 2 mm, which was calculated using Eq. (5). Moreover, the tube material in [49] was made of aluminum alloy A6061-T6 leading to $k = 0.15$ and $\eta = 0.75$ for our analytical analysis.

In Fig. 6 and Table 1, we provided a comparison between the theoretical predictions of our model and the experimental results. As shown in Fig. 6a, the analytical predictions of our model for UT tubes were in excellent agreement with the experimental results, with less than 6% error differences observed for the mean crushing force of UT tube.

In Fig. 6b, we present the changes in the crushing force of FGT tubes, and it is important to note that the force–displacement curves are only presented for the first 60 mm of displacement which is attributed to the deformation of the structure transitions from symmetric to asymmetric after 60 mm of displacement, based on the literature [47]. By limiting our analysis to the first 60 mm of displacement, we can accurately capture the symmetric deformation behavior of the structure and provide reliable predictions for the energy absorption performance of thin-walled structures under axial crushing.

By comparing the results of our proposed theoretical model with the experimental data, we observe that the theoretical

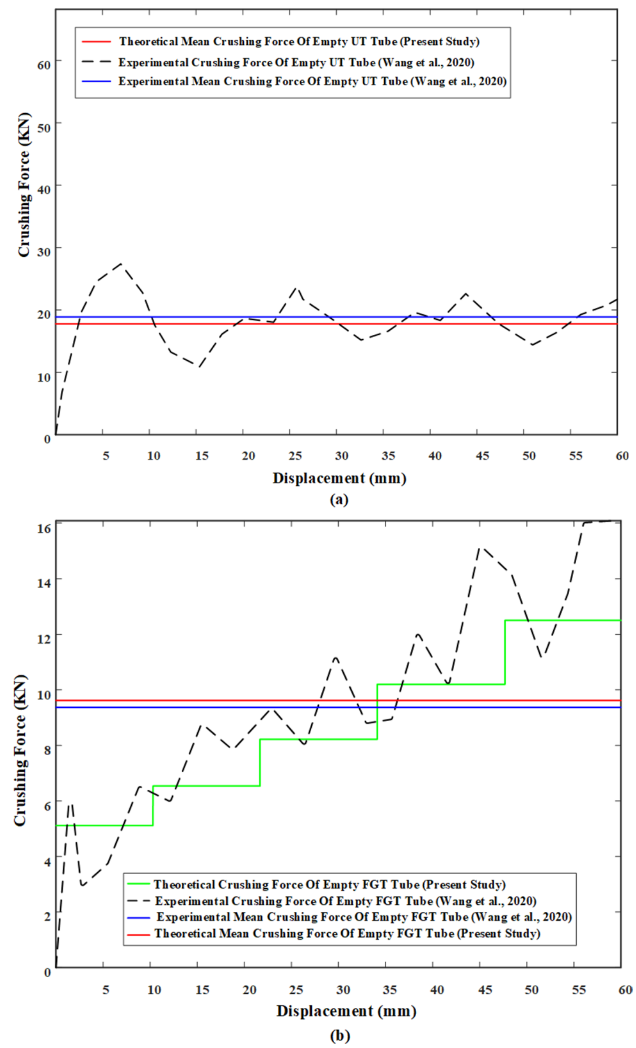

Fig. 6 Comparisons of present theoretical predictions with previous experimental results [49] for **a** E-UT tube; **b** E-FGT tube

Table 1 The comparisons of theoretical predictions with experimental results of ref. [49] for the mean crushing force of E-FGT and E-UT tubes

	Mean Crushing Force (KN)		
Tube Type	Experiment	Theory	Difference (%)
E-UT	18.86	17.78	-5.76
E-FGT	9.37	9.62	2.65

and experimental mean crushing forces and crushing forces of each fold are in good agreement. As depicted in Fig. 6b, both the theoretical and experimental results indicate that the crushing force required for each folding cycle in FGT tubes is greater than the crushing force of the previous folds. This observation highlights the importance of considering the local stiffness variations in FGT tubes when evaluating their energy

Table 2 Mechanical properties of foam material [32]

Density ρ_f (Kg/m^3)	Plateau stress σ_p (MPa)
270	1.8

Table 3 The comparisons of the theoretical predictions with experimental results [32] for the mean crushing force of F-UT tube

	Mean crushing force (KN)		
Tube type	Experiment	Theory	Difference (%)
F-UT	7.29	7.65	5.00

absorption performance. Table 1 summarizes the comparison between the theoretical predictions and the experimental results for the mean crushing force of E-FGT and E-UT tubes. By examining the mean crushing force of E-FGT tubes, we observed that the theoretical prediction aligns well with the experimental data, with the difference between analytical and experimental results being less than 3%. This level of agreement confirms the accuracy and robustness of our theoretical model in predicting the progressive folding behavior of E-UT and E-FGT circular tubes subjected to axial crushing force.

The validation of our theoretical model for the F-UT circular tube was conducted using experimental results from [32], which demonstrated the accuracy and reliability of our approach. To maintain the consistency with [32], we kept the geometrical parameters and material of the circular tube the same, with $R=31$ mm, $H=120$ mm, t = 0.8mm, and σ_0=59 Mpa. The UT tube used in [32] was made of aluminum alloy A6061-T6, and accordingly, we assumed an effective crushing distance factor η of 0.75 in our theoretical analysis. The foam material used in [32] is detailed in Table 2. Table 3 presents a comparative analysis of the theoretical predictions from our model and the experimental results from [32]. Our results demonstrate that in the case of the F-UT tube, the relative error in calculating the mean crushing force was only 5%, which indicates that our theoretical predictions are in excellent agreement with the experimental data [32].

As previously mentioned, while there have been several studies investigating the crushing behavior of FGT circular tubes under various loading conditions, there is a lack of experimental investigations into the crashing behavior of F-FGT circular tubes under axial compression, specifically with the appropriate material details and geometry. Despite this limitation, we can still confidently assume that the theoretical model proposed for F-FGT circular tubes will yield accurate results. This is because the theoretical model for F-FGT circular tubes shares similar assumptions with the validated theoretical model for F-UT circular tubes, which considers the energy absorbed by the foam material and the interaction between the tube wall and the foam filler. As a result, we can safely assume that the theoretical model proposed for F-FGT circular tubes will also produce reliable results. Although the absence of experimental data for F-FGT circular tubes may limit our ability to validate the theoretical model proposed in our study, the similarities between the theoretical models for F-UT and F-FGT circular tubes suggest that the proposed model will provide valuable insights into the energy absorption performance of thin-walled structures under axial compression. Moving forward, experimental investigations into the crashing behavior of F-FGT circular tubes with the appropriate material details and geometry would be beneficial for further validating and refining our theoretical model. Nonetheless, our findings provide valuable insights for designing more crashworthy structures that can enhance passenger safety and reduce the severity of vehicle collisions.

4.2 Comparison of E-UT and E-FGT circular tubes

In this section, the crushing behavior of E-FGT circular tubes for different normalized FGT tube wall thickness (t_{max}/t_{min}= 1.5, 2, 2.5 and 3) and grading exponents ($n=0.4$, 1 and 4) with axisymmetric deformation modes are investigated theoretically, and the results are compared with their E-UT counterparts. Aluminum alloy A6061-T6 was chosen as tube material, and the property of the material is provided in Table 4 [49]. In this section, SEA of E-FGT (SEA^{E-FGT}) and E-UT (SEA^{E-UT}) tubes were calculated at the crushing distance of 135mm (about 75% of the total height), and the results are shown in Table 5. In this theoretical analysis, the effective crushing distance factor η and the eccentricity factor m are taken 0.75 and 0.65, respectively. The results from Table 5 show that for different values of grading exponent (n) and normalized FGT tube wall thickness (t_{max}/t_{min}), E-FGT circular tubes exhibit a higher value of SEA compared to their corresponding E-UT counterparts, indicating superior crushing behavior of FGT circular tubes.

Figure 7 shows the relative difference of SEA between E-FGT and their E-UT counterparts for different values of normalized FGT tube wall thicknesses (t_{max}/t_{min}= 1.5, 2, 2.5, and 3) and grading exponents ($n=0.4$, 1, and 4). For n values of 1 and 4, we observed that increasing the normalized FGT tube wall thickness (t_{max}/t_{min}) results in a decrease

Table 4 Mechanical properties of the tube material [49]

Density, ρ_t (kg/m^3)	Young Modulus, E (GPa)	Yield Stress, σ_y (MPa)	Ultimate Stress, σ_u (MPa)	k
2700	70	100	125	0.15

Table 5 SEA of E-UT (SEA^{E-UT}) and E-FGT (SEA^{E-FGT}) circular tubes for different normalized FGT tube wall thickness (t_{max}/t_{min}= 1.5, 2, 2.5 and 3) and grading exponents (n = 0.4, 1 and 4)

Tube type	n	R (mm)	H (mm)	t_{min} (mm)	t_{max}/t_{min}	t_U (mm)	Total mass (g)	SEA^{E-FGT} (KJ/Kg)	SEA^{E-UT} (KJ/Kg)
E-FGT	0.4	30	180	1	1.5	1.357	124.3	14.2	10.7
					2	1.714	157.0	16.1	12.1
					2.5	2.071	189.7	17.8	13.3
					3	2.428	222.4	19.4	14.5
	1	30	180	1	1.5	1.250	114.5	13.6	10.2
					2	1.500	137.4	14.9	11.3
					2.5	1.750	160.3	16.2	12.2
					3	2.000	183.2	17.5	13.1
	4	30	180	1	1.5	1.100	100.7	12.5	9.6
					2	1.200	109.9	12.9	10.0
					2.5	1.300	119.0	13.2	10.4
					3	1.400	128.2	13.6	10.9

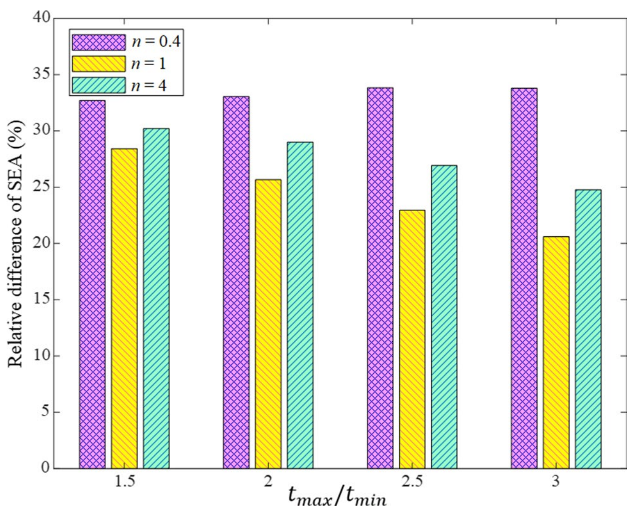

Fig. 7 The comparison of relative difference of SEA between E-FGT and their E-UT counterparts (relative difference $\% = \frac{SEA^{E-FGT} - SEA^{E-UT}}{SEA^{E-UT}} \times 100$)

in the relative difference of SEA between E-FGT and their E-UT counterparts as shown in Fig. 7a. However, for n = 0.4, we found that as the value of t_{max}/t_{min} increases from 1.5 to 2 and from 2 to 2.5, the relative difference of SEA between E-FGT and their E-UT counterparts increases. Interestingly, for t_{max}/t_{min}=2.5, we observed that the relative difference of SEA is smaller than that for t_{max}/t_{min}=2.

4.3 Effect of grading exponent n

In Fig. 8, it can be observed that the influence of different grading exponents (n) on the mean crushing force required to complete each folding cycle of E-FGT circular tubes with axisymmetric deformation modes, while maintaining constant values of the normalized wall thickness (t_{max}/t_{min}). In addition, the EA and SEA of the structures at a crushing distance of 135 mm were calculated and the results are presented in Table 6. The effective crushing distance factor (η), eccentricity factor (m), and tube material were consistent with those used in the previous section. All of the E-FGT tubes had a minimum thickness of 1 mm.

The analysis of Fig. 8 and Table 6 reveals significant insights into the relationship between the grading exponent and the mechanical behavior of functionally graded thin-walled tubes. Specifically, when considering a fixed value of normalized wall thickness (t_{max}/t_{min}), an increase in the grading exponent from 0.4 to 4 leads to a noteworthy reduction in both the mean crushing force required for each folding cycle and the total energy absorbed by the structure during deformation. Additionally, this increase in the grading exponent results in a decrease in the mass of the structure.

These findings can be attributed to the underlying changes in the wall thickness pattern of the tubes as the grading exponent increases. Figure 3 demonstrates that as the grading exponent rises from 0.4 to 4, the wall thickness pattern transforms from convex to concave. This alteration in the wall thickness distribution significantly affects the structural response during crushing.

4.4 Effect of normalized wall thickness t_{max}/t_{min}

In this section, the impact of normalized wall thickness (t_{max}/t_{min}) on the crushing behavior of the structures at constant values of grading exponent was investigated, and the results were presented in Fig. 9 and Table 7. The tube material used in this analysis is the same as in the previous sections, and the details related to the geometry of each structure are provided in Table 7. According to Fig. 9, for any given value of grading exponent, increasing the normalized wall thickness (t_{max}/t_{min}) leads to an increased difference between the MCF of each cycle compared to the previous ones. However, as the grading exponent increases, the effect

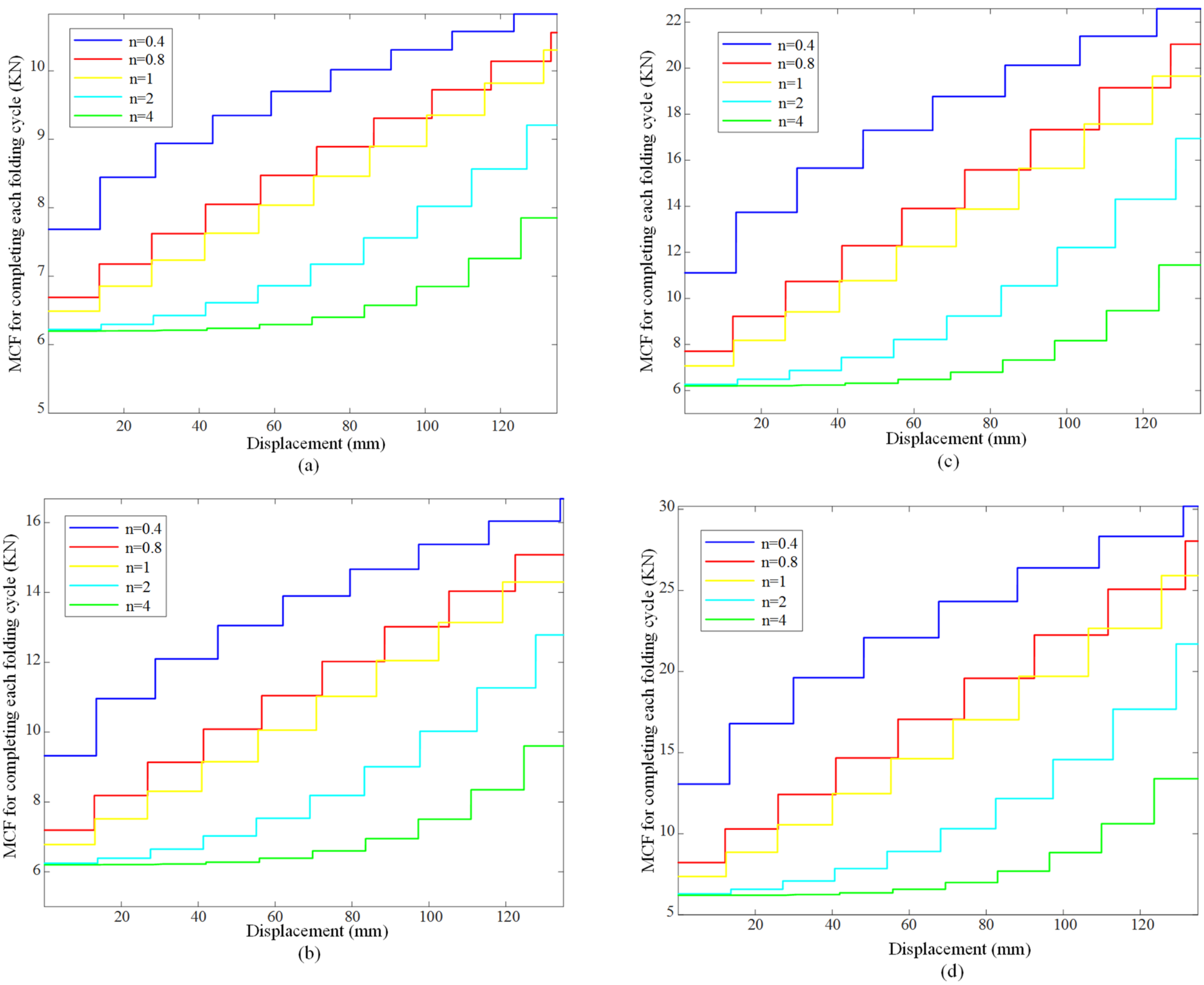

Fig. 8 The effect of different values of grading exponent n on the MCF necessary for completing each folding cycle for **a** t_{max}/t_{min} = 1.5; **b** t_{max}/t_{min} = 2; **c** t_{max}/t_{min} = 2.5; **d** t_{max}/t_{min} = 3

of normalized wall thickness on the mean crushing force required to complete elementary folding cycles of the structure during axial compression decreases. For example, in the case of $n=8$, the difference between MCF of the structures with t_{max}/t_{min}=1.5 and 2.5 is small and can be neglected in the first 55 mm displacement of the structure.

Table 7 provides crucial insights into the total energy absorption (EA) and specific energy absorption (SEA) of the examined structures at a crushing distance of 135mm. The findings indicate that when the grading exponent remains constant, an increase in the normalized wall thickness leads to a notable rise in the total mass, energy absorption (EA), and specific energy absorption (SEA) of the structure, as demonstrated in Table 7. However, an intriguing observation emerges as the grading exponent is increased. It is evident that any variations in the normalized wall thickness (t_{max}/t_{min}) have a diminishing impact on the total mass, energy absorption (EA), and specific energy absorption (SEA) of the E-FGT structures. In other words, as the grading exponent increases, the influence of changes in the normalized wall thickness becomes less pronounced. These findings provide compelling evidence that the grading exponent plays a critical role in determining the overall performance characteristics of the structures. While variations in the normalized wall thickness have a significant impact at lower grading exponents, this effect diminishes with higher grading exponents. This suggests that the structural behavior becomes more resilient and less sensitive to changes in the wall thickness pattern as the grading exponent increases.

Table 6 EA and SEA of E-FGT circular tubes for different normalized wall thickness (t_{max}/t_{min}= 1.5, 2, 2.5, and 3) and grading exponents (n = 0.4, 0.8, 1, 2, and 4)

Tube type	R (mm)	H (mm)	t_{min} (mm)	t_{max}/t_{min}	n	Total mass (g)	EA (KJ)	SEA^{E-FGT} (KJ/kg)
E-FGT	30	180	1	1.5	0.4	124.3	1.2886	14.2
					0.8	117.0	1.1522	13.7
					1	114.5	1.1061	13.6
					2	106.8	0.9749	13.0
					4	100.7	0.8865	12.5
	30	180	1	2	0.4	157.0	1.8085	16.1
					0.8	142.5	1.5101	15.2
					1	137.4	1.4076	14.9
					2	122.1	1.1269	13.8
					4	109.9	0.9393	12.9
	30	180	1	2.5	0.4	189.7	2.3934	17.8
					0.8	167.9	1.9068	16.7
					1	160.3	1.7435	16.2
					2	137.4	1.2920	14.7
					4	119.0	0.9951	13.2
	30	180	1	3	0.4	222.4	3.0330	19.4
					0.8	193.4	2.3365	18.1
					1	183.2	2.1088	17.5
					2	152.6	1.4697	15.6
					4	128.2	1.0539	13.6

4.5 Foam filling effect

In an F-FGT tube, the interaction energy between the tube wall and foam material can be described by two dimensionless functions of the eccentricity factor (m), denoted as the interaction coefficients $C_1(m)$ and $C_2(m)$. Figure 10 illustrates the relationship between the eccentricity factor (m) and these coefficients. As the eccentricity factor (m) increases from 0 to 1, the first coefficient of interaction ($C_1(m)$) decreases from its maximum value (π) to its minimum value (0), as depicted in Fig. 10. Conversely, the second coefficient of interaction ($C_2(m)$) exhibits an increase from 1.333 to 1.785 as the eccentricity factor (m) increases from 0 to 0.1532, reaching its maximum value. However, further increasing the eccentricity factor (m) beyond 0.1532 causes $C_2(m)$ to decrease, eventually reaching its minimum value of 0. Consequently, as the eccentricity factor (m) increases, the energy dissipated by the interaction diminishes. When the eccentricity factor (m) equals 1, the interaction energy becomes 0, indicating that it no longer influences the total energy absorbed by the F-FGT tube.

Table 8 shows that the SEA of F-FGT circular tubes for different normalized FGT tube wall thickness (t_{max}/t_{min}= 1.25, 1.5, 1.75, and 2) and grading exponents (n = 0.4, 1 and 4) with axisymmetric deformation modes, and the results were compared with their F-UT counterparts. The tube material and the foam filler material were similar to those of [49], and SEA of F-FGT (SEA^{F-FGT}) and F-UT (SEA^{F-UT}) tubes were calculated at the crushing distance of 135mm. Table 8 shows that all of the F-FGT circular tubes had a higher value of specific energy absorption (SEA) than their corresponding F-UT counterparts. As a result, the crushing behavior of F-FGT circular tubes was superior to that of their F-UT counterparts. Additionally, it was observed that for any constant value of grading exponent, increasing the normalized FGT tube wall thickness (t_{max}/t_{min}) led to an increase in the SEA of both F-FGT and F-UT tubes, improving the crushing behavior of the structures during axial compression.

5 Conclusions

In this study, we have introduced a novel theoretical model based on the concept of super folding elements to analyze the axisymmetric deformation of empty and foam-filled FGT circular tubes with different thickness patterns. The accuracy of the model was validated against previous experimental results, leading to the following significant conclusions:

1. Accurate Prediction of Axial Crushing Behavior: The proposed model demonstrates precise predictions of the axial crushing behavior for both empty and foam-filled FGT and UT circular tubes under axisymmetric deformation.

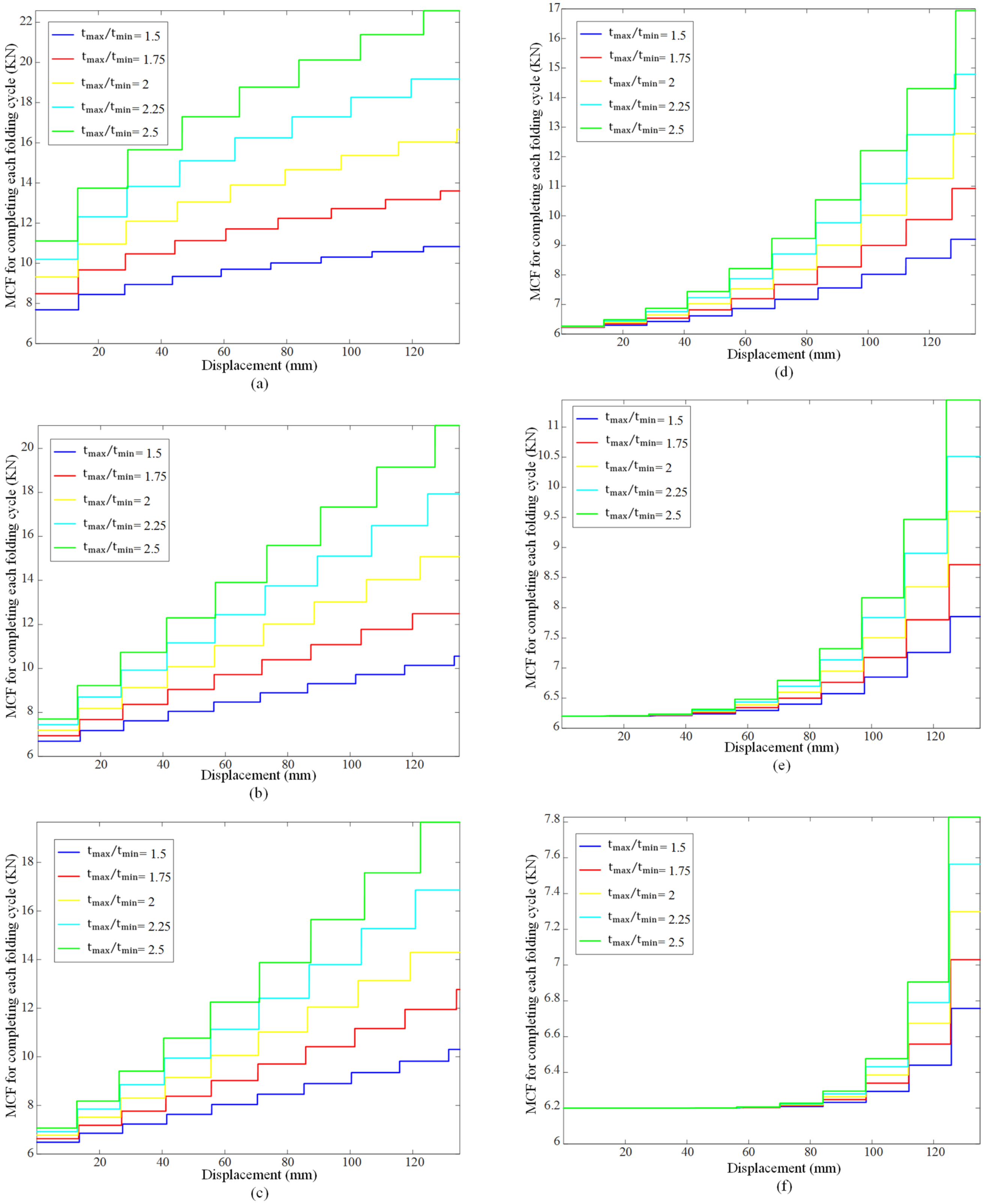

Fig. 9 The effect of different values of normalized wall thickness t_{max}/t_{min} on the MCF necessary for completing each folding cycle for **a** $n=0.4$; **b** $n=0.8$; **c** $n=1$; **d** $n=2$; **e** $n=4$ and **f** $n=8$

Table 7 EA and SEA of E-FGT circular tubes for different normalized wall thickness (t_{max}/t_{min}= 1.5, 1.75, 2, 2.25, and 2.5) and grading exponents (n=0.4, 0.8, 1, 2, 4, and 8)

Tube type	R (mm)	H (mm)	t_{min} (mm)	n	t_{max}/t_{min}	Total mass (g)	EA (KJ)	SEA^{E-FGT} (KJ/Kg)
E-FGT	30	180	1	0.4	1.50	124.3	1.2886	14.22
					1.75	140.6	1.5409	15.17
					2.00	157.0	1.8085	16.08
					2.25	173.4	2.0933	16.96
					2.50	189.7	2.3934	17.81
	30	180	1	0.8	1.50	117.0	1.1522	13.73
					1.75	129.7	1.3256	14.49
					2.00	142.5	1.5100	15.24
					2.25	155.2	1.7040	15.98
					2.50	167.9	1.9068	16.69
	30	180	1	1	1.50	114.5	1.1061	13.55
					1.75	125.9	1.2526	14.22
					2.00	137.4	1.4076	14.89
					2.25	148.8	1.5717	15.57
					2.50	160.3	1.7435	16.24
	30	180	1	2	1.50	106.8	0.9749	12.97
					1.75	114.5	1.0492	13.38
					2.00	122.1	1.1269	13.81
					2.25	129.7	1.2078	14.24
					2.50	137.4	1.2920	14.67
	30	180	1	4	1.50	100.7	0.8865	12.50
					1.75	105.3	0.9125	12.68
					2.00	109.9	0.9393	12.85
					2.25	114.5	0.9668	13.04
					2.50	119.0	0.9951	13.22
	30	180	1	8	1.50	96.6	0.8473	12.26
					1.75	99.2	0.8526	12.30
					2.00	101.7	0.8578	12.34
					2.25	104.3	0.8631	12.39
					2.50	106.8	0.8684	12.43

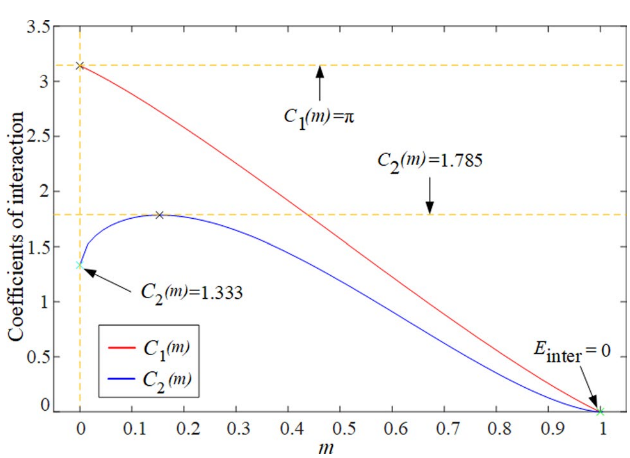

Fig. 10 The change of interaction coefficients $C_1(m)$ and $C_2(m)$ with the eccentricity factor m

2. Enhanced Energy Absorption in Empty FGT Tubes: We observed that empty FGT circular tubes exhibit a higher specific energy absorption (SEA) compared to their empty UT counterparts for values of $0.4 < n < 4$.
3. Optimal Design Scheme for Empty FGT Tubes: Empty FGT structures with smaller grading exponents exhibit greater energy absorption (EA) and specific energy absorption (SEA) at any constant value of the normalized wall thickness (t_{max}/t_{min}). Hence, empty FGT structures are considered the optimal choice as energy absorbers, showcasing more ideal energy absorption behavior.
4. Influence of Normalized Wall Thickness on Energy Absorption: By increasing the normalized wall thickness (t_{max}/t_{min}) of empty FGT circular tubes for any given grading exponent, we observed higher values of energy absorption (EA) and specific energy absorption (SEA) within the structure.

Table 8 EA and SEA of F-FGT circular tubes for different normalized wall thicknesses (t_{max}/t_{min}= 1.25, 1. 5, 1.75, and 2) and grading exponents (n=0.4, 1, and 4)

Tube Type	n	R (mm)	H (mm)	σ_P (MPa)	t_{min} (mm)	t_{max}/t_{min}	t_U (mm)	Tube mass (g)	Foam mass (g)	SEA^{F-FGT} (KJ/kg)	SEA^{F-UT} (KJ/kg)
F-FGT	0.4	33	180	1.8	1.5	1.25	1.767	178.1	157.4	11.9	8.9
						1.50	2.035	205.1	156.1	12.8	9.7
						1.75	2.303	232.1	154.8	13.8	10.4
						2.00	2.571	259.1	153.5	14.7	11.1
	1	33	180	1.8	1.5	1.25	1.687	170.0	157.8	11.5	8.7
						1.50	1.875	188.9	156.9	12.1	9.2
						1.75	2.062	207.8	156.0	12.8	9.7
						2.00	2.250	226.7	155.1	13.4	10.3
	4	33	180	1.8	1.5	1.25	1.575	158.7	158.4	11.0	8.4
						1.50	1.650	166.2	158.0	11.2	8.6
						1.75	1.725	173.8	157.6	11.3	8.8
						2.00	1.800	181.3	157.3	11.5	9.0

5. Interaction Energy in Foam-Filled FGT Tubes: The amount of energy absorbed due to the interaction between the tube wall and the foam-filler depends on the interaction coefficients $C_1(m)$ and $C_2(m)$. For cases where $m = 1$, the interaction coefficients $C_1(m)$ and $C_2(m)$ become zero, indicating no interaction between the foam-filler and the tube wall. Therefore, the interaction energy can be disregarded in foam-filled FGT circular tubes.
6. Superior Energy Absorption in Foam-Filled FGT Tubes: Foam-filled FGT circular tubes exhibit higher specific energy absorption (SEA) compared to their foam-filled UT counterparts for any given values of grading exponents ($0.4 < n < 4$). This finding highlights that foam-filled FGT circular tubes are superior candidates as energy-absorbing structures.

In summary, our study presents a high-level generalization and summary of the main work conducted in this paper. It also provides insights into the best design scheme for structural design, emphasizing the superior energy absorption capabilities of empty and foam-filled FGT circular tubes. Furthermore, the potential application value of the proposed theoretical model is clarified by demonstrating its effectiveness in accurately predicting axial crushing behavior and guiding the optimal design of energy-absorbing structures.

Funding No funding was received to assist with the preparation of this manuscript.

Declarations

Conflict of interest The authors have no conflict of interest to declare that are relevant to the content of this article.

References

1. Ahmad Z, Thambiratnam DP (2009) Application of foam-filled conical tubes in enhancing the crashworthiness performance of vehicle protective structures. Int J Crashworthiness 14(4):349–363
2. Bisagni C (2002) Crashworthiness of helicopter subfloor structures. Int J Impact Eng 27(10):1067–1082
3. Wang Z et al (2017) Mechanical behavior of composited structure filled with tandem honeycombs. Compos B Eng 114:128–138
4. Wang Z et al (2016) Matching effect of honeycomb-filled thin-walled square tube—experiment and simulation. Compos Struct 157:494–505
5. Abramowicz W, Jones N (1984) Dynamic axial crushing of square tubes. Int J Impact Eng 2(2):179–208
6. Abramowicz W, Jones N (1984) Dynamic axial crushing of circular tubes. Int J Impact Eng 2(3):263–281
7. Abramowicz W, Jones N (1986) Dynamic progressive buckling of circular and square tubes. Int J Impact Eng 4(4):243–270
8. Yao R, Zhang B, Yin G, Zhao Z (2020) Energy absorption behaviors of foam-filled holed tube subjected to axial crushing: experimental and theoretical investigations. Mech Adv Mater Struct 28(24):501–2514
9. Niknejad A et al (2012) Prediction of the mean folding force during the axial compression in foam-filled grooved tubes by theoretical analysis. Mater Des 37:144–151
10. Abedi MM et al (2018) Foam-filled grooved tubes with circular cross section under axial compression: an experimental study. Iran J Sci Technol Trans Mech Eng 42(4):401–413
11. VimalKannan I, Rajkumar R (2020) Deformation and energy absorption analysis of simple and multi-cell thin-walled tubes under quasi-static axial crushing. Int J Crashworthiness 25(2):121–130
12. Jin M et al (2022) Improving the crashworthiness of bio-inspired multi-cell thin-walled tubes under axial loading: experimental, numerical, and theoretical studies. Thin-Walled Struct 177:109415
13. Nagel G, Thambiratnam D (2004) A numerical study on the impact response and energy absorption of tapered thin-walled tubes. Int J Mech Sci 46(2):201–216
14. Reid S, Reddy T (1986) Static and dynamic crushing of tapered sheet metal tubes of rectangular cross-section. Int J Mech Sci 28(9):623–637

15. Mamalis A, Johnson W (1983) The quasi-static crumpling of thin-walled circular cylinders and frusta under axial compression. Int J Mech Sci 25(9–10):713–732
16. Guillow S, Lu G, Grzebieta R (2001) Quasi-static axial compression of thin-walled circular aluminium tubes. Int J Mech Sci 43(9):2103–2123
17. Ebrahimi S, Vahdatazad N, Liaghat G (2018) Experimental characterization of the energy absorption of functionally graded foam filled tubes under axial crushing loads. J Theor Appl Mech 48(1):76
18. Hong W et al (2013) Quasi-static axial compression of triangular steel tubes. Thin-Walled Struct 62:10–17
19. Abedi MM et al (2012) Theoretical and experimental study on empty and foam-filled columns with square and rectangular cross section under axial compression. Int J Mech Sci 65(1):134–146
20. Gao Z et al (2023) Axial compression of multi-cell hexagonal tubes with novel hierarchical architectures: numerical and theoretical analyses. Compos Struct 318:117079
21. Yang F, Deng X, Wang C (2023) Analysis of energy absorption characteristics of a sinusoidal corrugated filled tube. Mech Adv Mater Struct. https://doi.org/10.1080/15376494.2023.2244961
22. Liu W et al (2016) Dynamic performances of thin-walled tubes with star-shaped cross section under axial impact. Thin-Walled Struct 100:25–37
23. de Lemos Coutinho L et al (2022) Energy absorption of CFRP composite thin-walled tubes with PVC foam-filled cores. Innov Infrastruct Solut 7(2):168
24. Yang H, Lei H, Lu G (2021) Crashworthiness of circular fiber reinforced plastic tubes filled with composite skeletons/aluminum foam under drop-weight impact loading. Thin-Walled Struct 160:107380
25. AlGalib D, Limam A (2004) Experimental and numerical investigation of static and dynamic axial crushing of circular aluminum tubes. Thin-Walled Struct 42(8):1103–1137
26. Simhachalam B, Srinivas K, Rao CL (2014) Energy absorption characteristics of aluminium alloy AA7XXX and AA6061 tubes subjected to static and dynamic axial load. Int J Crashworthiness 19(2):139–152
27. Marzbanrad J, Ebrahimi MR (2011) Multi-objective optimization of aluminum hollow tubes for vehicle crash energy absorption using a genetic algorithm and neural networks. Thin-Walled Struct 49(12):1605–1615
28. Wang Z, Liu J (2018) Mechanical performance of honeycomb filled with circular CFRP tubes. Compos B Eng 135:232–241
29. Liu J, Wang Z, Hui D (2018) Blast resistance and parametric study of sandwich structure consisting of honeycomb core filled with circular metallic tubes. Compos B Eng 145:261–269
30. Liu W et al (2018) Crashworthiness analysis of cylindrical tubes filled with conventional and negative Poisson's ratio foams. Thin-Walled Struct 131:297–308
31. Meguid S, Cheon S, El-Abbasi N (2002) FE modelling of deformation localization in metallic foams. Finite Elem Anal Des 38(7):631–643
32. Yang F, Fan H, Meguid S (2019) Effect of foam-filling on collapse mode transition of thin-walled circular columns under axial compression: analytical, numerical and experimental studies. Int J Mech Sci 150:665–676
33. Hanssen AG, Langseth M, Hopperstad OS (2000) Static and dynamic crushing of square aluminium extrusions with aluminium foam filler. Int J Impact Eng 24(4):347–383
34. Hanssen AG, Langseth M, Hopperstad OS (2000) Static and dynamic crushing of circular aluminium extrusions with aluminium foam filler. Int J Impact Eng 24(5):475–507
35. Yang F, Meguid S, Hamouda A (2018) Kinematically admissible folding mechanisms for the progressive collapse of foam filled conical frusta. Int J Mech Mater Des 14(1):105–126
36. Pan F, Zhu P, Zhang Y (2010) Metamodel-based lightweight design of B-pillar with TWB structure via support vector regression. Comput Struct 88(1–2):36–44
37. Xu F et al (2013) Crashworthiness design of multi-component tailor-welded blank (TWB) structures. Struct Multidiscip Optim 48(3):653–667
38. Xu P et al (2016) Crash performance and multi-objective optimization of a gradual energy-absorbing structure for subway vehicles. Int J Mech Sci 107:1–12
39. Pan F, Zhu P (2011) Lightweight design of vehicle front–end structure: contributions of multiple surrogates. Int J Veh Des 57(2–3):124–147
40. Meyer A, Wietbrock B, Hirt G (2008) Increasing of the drawing depth using tailor rolled blanks—numerical and experimental analysis. Int J Mach Tools Manuf 48(5):522–531
41. Chuang C et al (2008) Multidisciplinary design optimization on vehicle tailor rolled blank design. Struct Multidiscip Optim 35(6):551–560
42. Urban M et al (2006) Numerical research and optimisation of high pressure sheet metal forming of tailor rolled blanks. J Mater Process Technol 177(1–3):360–363
43. Sun G et al (2014) Crashing analysis and multiobjective optimization for thin-walled structures with functionally graded thickness. Int J Impact Eng 64:62–74
44. Li G et al (2015) A comparative study on thin-walled structures with functionally graded thickness (FGT) and tapered tubes withstanding oblique impact loading. Int J Impact Eng 77:68–83
45. Zhang X, Zhang H, Wen Z (2015) Axial crushing of tapered circular tubes with graded thickness. Int J Mech Sci 92:12–23
46. Yao S, Xing Y, Zhao K (2017) Crashworthiness analysis and multiobjective optimization for circular tubes with functionally graded thickness under multiple loading angles. Adv Mech Eng 9(4):1687814017696660
47. Baykasoglu C, Cetin MT (2015) Energy absorption of circular aluminium tubes with functionally graded thickness under axial impact loading. Int J Crashworthiness 20(1):95–106
48. Sun G et al (2017) Energy absorption mechanics for variable thickness thin-walled structures. Thin-Walled Struct 118:214–228
49. Wang P et al (2020) Energy absorption of thin-walled circular tubes with gradient thickness under oblique loads. Proc Inst Mech Eng C J Mech Eng Sci 234(16):3207–3220
50. Zhang H, Gao Z, Ruan D (2023) Square tubes with graded wall thickness under oblique crushing. Thin-Walled Struct 183:110429
51. Sun G et al (2010) Crashworthiness design for functionally graded foam-filled thin-walled structures. Mater Sci Eng A 527(7–8):1911–1919
52. Guler MA et al (2010) The effect of geometrical parameters on the energy absorption characteristics of thin-walled structures under axial impact loading. Int J Crashworthiness 15(4):377–390
53. Wierzbicki T et al (1992) Alexander revisited—a two folding elements model of progressive crushing of tubes. Int J Solids Struct 29(24):3269–3288
54. Abramowicz W, Wierzbicki T (1988) Axial crushing of foam-filled columns. Int J Mech Sci 30(3–4):263–271
55. Meguid S, Yang F, Verberne P (2015) Progressive collapse of foam-filled conical frustum using kinematically admissible mechanism. Int J Impact Eng 82:25–35
56. Rahi A (2019) Experimental and crash-worthiness optimization of end-capped conical tubes under quasi-static and dynamic loading. Mech Adv Mater Struct 26(17):1437–1446

57. Abramowicz W (1983) The effective crushing distance in axially compressed thin-walled metal columns. Int J Impact Eng 1(3):309–317

Publisher's Note Springer Nature remains neutral with regard to jurisdictional claims in published maps and institutional affiliations.